THE JOURNAL OF PHYSICAL CHEMISTRY LETTERS
A JOURNAL OF THE AMERICAN CHEMICAL SOCIETY

pubs.acs.org/JPCL

Letter

Ultrafast Proton Transfer Pathways Mediated by Amphoteric Imidazole

Marius-Andrei Codescu, Thomas Kunze, Moritz Weiß, Martin Brehm, Oleg Kornilov, Daniel Sebastiani,* and Erik T. J. Nibbering*

Cite This: *J. Phys. Chem. Lett.* 2023, 14, 4775−4785

Read Online

ACCESS | Metrics & More | Article Recommendations | Supporting Information

ABSTRACT: Imidazole, being an amphoteric molecule, can act both as an acid and as a base. This property enables imidazole, as an essential building block, to effectively facilitate proton transport in high-temperature proton exchange membrane fuel cells and in proton channel transmembrane proteins, enabling those systems to exhibit high energy conversion yields and optimal biological function. We explore the amphoteric properties of imidazole by following the proton transfer exchange reaction dynamics with the bifunctional photoacid 7-hydroxyquinoline (7HQ). We show with ultrafast ultraviolet-mid-infrared pump−probe spectroscopy how for imidazole, in contrast to expectations based on textbook knowledge of acid−base reactivity, the preferential reaction pathway is that of an initial proton transfer from 7HQ to imidazole, and only at a later stage a transfer from imidazole to 7HQ, completing the 7HQ tautomerization reaction. An assessment of the molecular distribution functions and first-principles calculations of proton transfer reaction barriers reveal the underlying reasons for our observations.

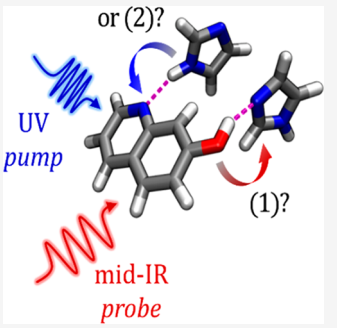

Amphoterism is the ability of molecules to act both as an acid and as a base. An example is water (H_2O) that can both donate a proton, becoming a hydroxide anion (OH^-), and accept a proton, forming the hydronium ion (H_3O^+). In a similar way, amphoterism governs the acid and base properties of other protic solvents such as alcohols (ROH) and amines (RNH_2) and heterocyclic aromatic molecular systems like imidazole ($C_3N_2H_4$). Another example is offered by ampholytes, molecules that have both acidic and basic groups, such as the amino acid H_2N-RCH-CO_2H, where tautomerism between a neutral form and a zwitterionic form is augmented with additional anionic and cationic forms. Amphoterism efficiently facilitates proton transport pathways by consecutive proton exchange steps, making it a key factor in the underlying microscopic mechanism of the von Grotthuss mechanism in water[1−9] and in other protic solvents.[10,11] In the von Grotthuss picture, the excess proton "jumps" sequentially along the solvent molecules at a pace much faster than what the Stokes−Einstein hydrodynamic diffusion model predicts for an individual protonated solvent molecule. Proton exchange is also understood to occur in a sequential von Grotthuss-like fashion in acid dissociation[12−16] and in acid−base neutralization reactions in protic solvents,[17−22] as well as for proton transport in phosphoric acid,[23] imidazole,[24] and imidazole derivatives.[25,26] Imidazole derivatives can be major constituents in hydrogen fuel cells,[27,28] for instance, as excellent proton carriers in high-temperature proton exchange membrane fuel cells (HT-PEMFC).[29] Finally, imidazole, being the functional group of the amino acid histidine, is a crucial building block in numerous biological systems, efficiently enabling energy transport,[30] signal transduction,[31] or pH regulation.[32−34]

In this Letter, we report our findings for imidazole as a means for ultrafast proton transport in a methanol solution. The reasons behind the particular choice of the two molecular compounds (methanol and imidazole) for the proton-conducting material are possibly not immediately obvious. In the context of (industrial) proton exchange membrane fuel cells, liquid water is a very common choice as the proton conductor, and in practice, it is realized in the form of water channels in an otherwise hydrophobic polymer matrix with sulfonic acid end groups (the famous NAFION material concept). These materials reach their functional limits at the boiling point of liquid water, which is why considerable effort is being dedicated to finding water-free proton-conducting materials. In contrast to water as such, midsized organic molecules (such as imidazole and hydroxylated alkanes) could be attached directly as side chains to the polymer backbone, which would reduce or eliminate the functional degradation due to evaporation at increased temperatures. In our experimental and computational setup, a direct consideration of polymers is not possible, which is why we resort to the corresponding molecular systems. The vision is that learning the local mechanisms of protonation dynamics in these

Received: March 3, 2023
Accepted: April 26, 2023
Published: May 15, 2023

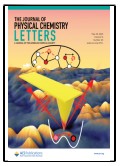

https://doi.org/10.1021/acs.jpclett.3c00595
J. Phys. Chem. Lett. 2023, 14, 4775−4785

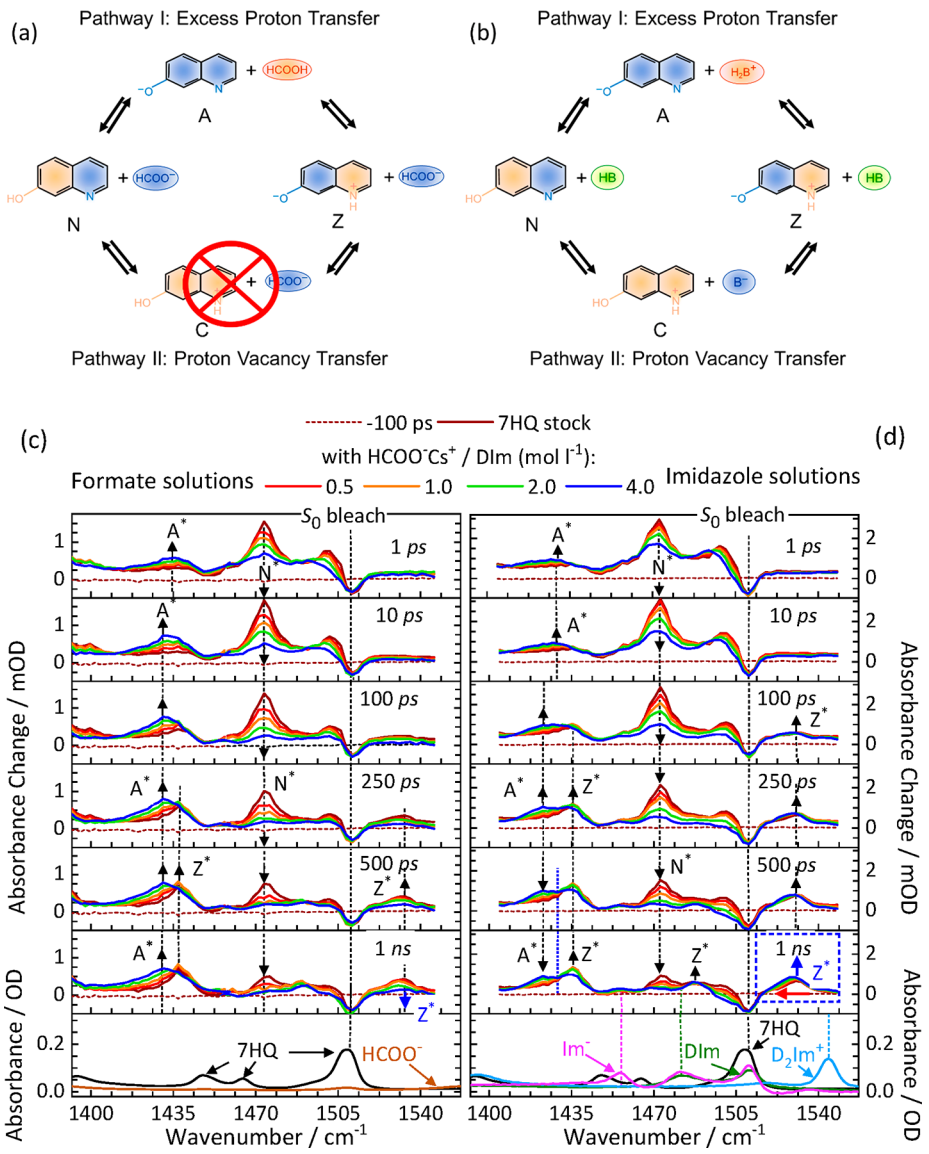

Figure 1. Comparison of the acid−base reaction pathways between the N and Z tautomers and the ionic A and C species of 7HQ, reacting with (a) formate ion/formic acid or (b) the amphoteric $H_2B^+/HB/B^-$, where HB can be imidazole, or the solvent H_2O or CH_3OH. Excess proton transfer pathway I can occur with the bases formate anion and imidazole but also with the solvent reacting with 7HQ. Note that for formate solutions proton vacancy pathway II can occur only with 7HQ exclusively reacting with the solvent, not with formate as the active reaction partner, whereas for imidazole solutions, both pathways are possible for imidazole and the solvent reacting with 7HQ. The transient UV-pump-IR-probe spectra are shown as a function of the base added to the deuterated methanol solution at particular pulse delay times for 7HQ reacting with (c) the formate anion or (d) imidazole. The dashed lines in the plots indicate the transient response recorded at −100 ps, showing the baseline in these measurements.

materials will enable or improve the rational design of real (polymeric) water-free proton-conducting materials.

For our purposes, we use 7-hydroxyquinoline (7HQ) to initiate proton transfer reactions and follow the dynamics using femtosecond UV-pump-IR-probe spectroscopy. The objective is to measure the reaction dynamics of "tight" contact and "loose" solvent-separated reaction pairs that can be prepared under well-defined conditions. The underlying mechanisms of proton transfer dynamics of such "tight" and "loose" photoacid−carboxylate complexes have been found to occur on time scales of hundreds of femtoseconds and several picoseconds, respectively. This difference in time scales is understood to be due to a single-step event with possible solvent shell rearrangements in the case of "tight" reaction pairs,[35] whereas a sequential mechanism from a proton-donating photoacid via the water solvent bridge to the accepting base necessitates hydrogen bond rearrangements facilitating the proton hops along the water bridge.[17] As the reaction dynamics time scales of these "tight" and "loose" complexes are clearly distinct from those of the photoacid molecules reacting with base molecules after more extensive configurational and diffusional motions that will involve a large number of hydrogen bond and solvent shell rearrangements taking place on time scales of hundreds of picoseconds (or longer), the latter fraction has time-dependent characteristics that rather can be regarded as being due to reaction kinetics without providing detailed insight into the elementary steps that underlie the proton exchange.

Amphoterism is also at play in the acid−base equilibrium of 7-hydroxyquinoline (7HQ) in the electronic S_0 ground state

https://doi.org/10.1021/acs.jpclett.3c00595
J. Phys. Chem. Lett. 2023, 14, 4775−4785

for both aqueous and methanol solutions, where for an aqueous solution under neutral pH ∼7 conditions both the neutral (N) and zwitterionic (Z) tautomer occur quantitatively, at a low pH of <2 the cationic form C dominates, and at a high pH of >10 the anionic form A is formed (see Figure 1).[36,37] 7HQ is a so-called bifunctional photoacid, for which electronic excitation of the $S_0 \rightarrow S_1$ transition of the neutral 7HQ tautomer N makes the molecule both a photoacid and a photobase. The pK_a value of the OH group decreases by 8 units, making 7HQ a strong acid, whereas the pK_b value of the quinoline nitrogen site changes by 5 units, making 7HQ also a stronger base. These properties strongly dictate the acid−base behavior in the first electronic excited state and photoinduced proton transfer dynamics of 7HQ in protic solvents.[11,36−42]

Recent results obtained in a combined ultrafast infrared spectroscopic and ab initio quantum molecular dynamics study of 7HQ in water/methanol mixtures have shown that on a microscopic level proton transport takes place from the proton-accepting quinoline group to the proton-donating OH group via a methoxide/hydroxide transport mechanism on a time scale of tens to hundreds of picoseconds.[11] Via the addition of another acid or base, it is possible to change the preference of the proton transfer pathways from a hydrolysis/methanolysis (solvolysis) "proton vacancy" mechanism (with 7HQ following the N* → C* → Z* route) to a protolysis "excess proton" mechanism (with 7HQ transforming from N* → A* → Z*). Our first results were obtained with the formate anion, which promptly accepts the proton from the OH group of 7HQ upon electronic excitation of the bifunctional photoacid, when in the proximity of 7HQ under either "tight" contact reaction pair or "loose" solvent-separated reaction pair conditions.[43] Our results obtained with the formate anion as an additive did not support a full quantitative transformation of 7HQ following the N* → A* → Z* pathway. In this work, we report on the possible role of imidazole as a mediator in the different proton transport pathways that 7HQ can follow, as always with a close interplay with and or even direct involvement of the nearest solvent molecules. Here we will show that amphoterism is at play with imidazole, acting both as a proton acceptor and as a proton donor, as opposed to *N*-methylimidazole that has been used as base in proton transfer studies with 7-hydroxy-4-(trifluoromethyl)-1-coumarin.[44] In the case of amphoteric imidazole, one cannot a priori assume that the dominant reaction pathway of 7HQ changes from the solvolysis (methanolysis) to the protolysis pathway when imidazole is added to a solution of 7HQ in a methanol solution, as imidazole can be the active reaction partner of 7HQ in both possible acid−base reaction routes. Whereas empirical free energy−reactivity relationships will provide clear hints about this matter for "loose" 7HQ−imidazole reaction pairs, there is no straightforward assessment available for the "tight" 7HQ−imidazole reaction pairs that may be envisaged to be present in solutions with high imidazole concentrations, as proton transfer reactions for "tight" acid−base reaction pairs may well have a low reaction barrier or may even be barrierless.

We follow the ultrafast proton transfer dynamics between 7HQ and imidazole as a function of time upon electronic excitation of the neutral 7HQ tautomer N at 330 nm. By using ultrafast infrared spectroscopy, we can follow the dynamical behavior of the different forms of ampholyte 7HQ in the first electronic excited state, namely, N* and Z* tautomers and charged C* and A* species.[11,42,43] The IR-active normal modes specific to each species of 7HQ in the S_1 state have been identified and characterized,[42] allowing the acid−base reaction dynamics along the protolysis or solvolysis pathways in deuterated methanol (CD_3OD) to be distinctly followed[11] (see Figure 1) and steered.[43] Figure 1 also provides an overview of the transient UV/IR pump−probe spectra recorded for the 7HQ−imidazole pair at specific pulse delay times when particular steps along the possible proton transfer pathways are anticipated to occur. We show here the spectral region of 1390−1560 cm^{-1} where the marker bands for different charged and tautomer species of 7HQ can be most easily discerned (a broader spectral range is presented in the Supporting Information). N* has a strong IR-active transition at 1475 cm^{-1}; Z* displays two IR-active bands at 1440 and 1530 cm^{-1}, while A* appears with a broad band at 1430 cm^{-1} but is narrower and frequency downshifted to 1422 cm^{-1} at longer pulse delays. The pulse delay-dependent magnitudes of these marker bands are directly proportional to the transient population of the 7HQ species in the S_1 state. For comparison, the transient UV/IR pump−probe spectra are depicted with those of a previously reported experiment on the 7HQ−formate photoacid−base system[43] and the stock solution of 7HQ.[11,42]

The following observations on proton transfer dynamics of 7HQ, as grasped from the transient response of the IR-active marker bands of 7HQ obtained with imidazole as a base, are much like those realized with formate: (1) an initial decrease in the level of N* and the appearance of A* within the time resolution, (2) a further decrease in the level of N* and the appearance of more A* on the time scale of a few picoseconds, (3) the magnitudes of the early time components of the decrease in the level of N* and the increase in the level of A* increase with imidazole concentration, and (4) the magnitude of the N* marker band decreases further at longer time scales of hundreds of picoseconds, scaling with the base concentration and approaching zero for the highest base concentration used in these experiments (4.0 M).

Distinctly different behavior can also be deduced from the comparison between the 7HQ−imidazole and 7HQ−formate results at the high base concentration depicted in Figure 1. Whereas in the 7HQ−formate case the transient A* marker band indicates that the proton transfer kinetics predominantly halts at the A* anion, for the 7HQ−imidazole case the reaction proceeds further. The appearance of the Z* marker bands occurs on a time scale of hundreds of picoseconds, whereas the A* marker band has by then frequency downshifted from 1430 to 1422 cm^{-1} and diminished in spectral breadth, suggesting a decrease in the transient population of A* on this long time scale. The initial large spectral breadth and subsequent narrowing of IR-active marker bands on picosecond time scales have often been observed for ultrafast photoinduced reactions[45] and ascribed to initial excess vibrational excitation (i.e., the molecules with increased internal vibrational population numbers are "hot"), followed by vibrational cooling by energy dissipation to the solvent shell molecules. Such phenomena are typically observed for IR-active vibrational modes of chromophores undergoing photoinduced chemical reactions. As anharmonic coupling constants have typically a negative sign, the IR-active fingerprint of initial "hot" molecules appears to be frequency downshifted, and with the vibrational cooling process, the spectral narrowing of the IR-active fingerprint modes is accompanied by a frequency upshift. However, in the case of 7HQ reacting with imidazole,

https://doi.org/10.1021/acs.jpclett.3c00595
J. Phys. Chem. Lett. 2023, 14, 4775−4785

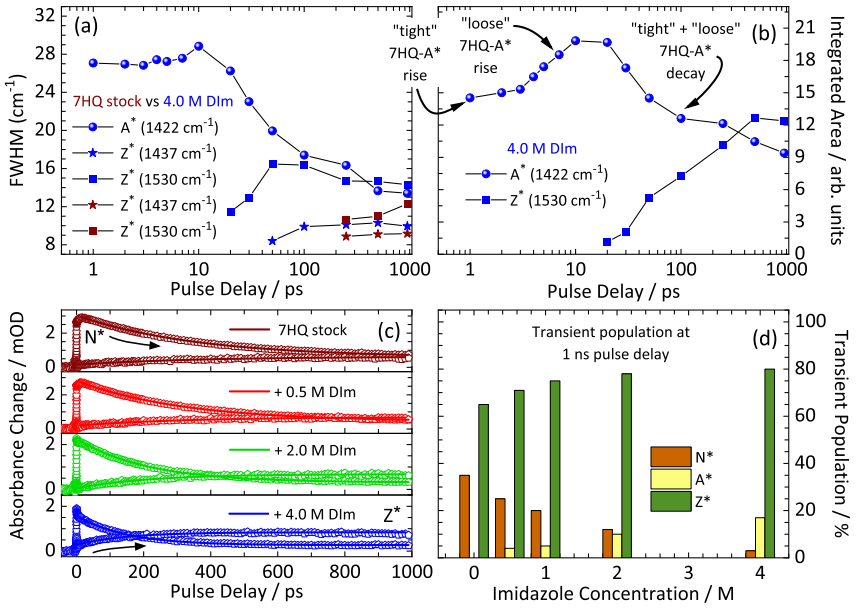

Figure 2. (a) Full widths at half-maximum (fwhm) of 7HQ marker bands for the A* and Z* species as a function of pulse delay time for the 7HQ stock and 4 M imidazole solutions. (b) Integrated areas of the A* and Z* marker bands (at 1422 and 1530 cm^{-1}, respectively), as a function of pulse delay time. (c) Transient kinetics of the 7HQ N* and Z* tautomers as a function of the DIm imidazole concentration. (d) Absolute population fractions of the N* and Z* tautomers and the A* anion at a 1 ns pulse delay time, derived from the transient UV/IR pump−probe spectra, as a function of imidazole concentration. Note that the curves depicted in panels a and b are shown with logarithmic scaling of the *x*-axis, whereas in panel c, a normal scaling has been used, to highlight the early time components of "tight" and "loose" complexes in panels a and b and the long time components in panel c.

the frequency shift occurs in the opposite direction. An alternative explanation for our observations on the A* marker band around 1422−1430 cm^{-1} on a time scale from picoseconds to several tens of picoseconds may be found in a possible distribution of hydrogen bond configurations directly upon proton/deuteron transfer from 7HQ to imidazole, converting N* into A*, followed by hydrogen bond and solvent shell rearrangements. Instead, the two marker bands of Z* at 1440 and 1530 cm^{-1} exhibit a small increase of spectral width with a large pulse delay for a high imidazole concentration compared to what has been observed for 7HQ without an added base. The 1470 cm^{-1} marker band of the N* species of 7HQ shows a small increase in spectral width but negligible changes in frequency position with an increase in imidazole concentration. Even though a normal mode analysis of the fingerprint modes of the four different 7HQ species, N*, C*, A*, and Z*, has been performed[42] and these normal modes have been found to be predominantly governed by C−C, C═C, C−N, and C═N stretching displacements of the C and N atoms in the aromatic quinoline ring parts and C−H bending motions of 7HQ, a proper analysis of the role of hydrogen bonding and solvent shell rearrangements can be performed only when the first solvent shell molecules are also included in these normal mode characterizations. Only further in-depth mode analysis of the IR-active marker vibrations of N*, A*, and Z* as well as an assessment of the distribution of the configurations of the 7HQ−imidazole reaction pairs and their temporal characteristics, which can be grasped by ab initio molecular dynamics simulations, may shed light on the underlying reasons for this interesting observation.

Whereas in our earlier studies[11,42] we have been able to successfully analyze the observed transient population kinetics by the time-dependent magnitude of the N*, A*, and Z* species, we found here that this approach has led to inconsistent results. The reason is that in these previous studies the population kinetics predominantly occurred on longer time scales of hundreds of picoseconds, whereas possible changes in the band shape and shifts in frequency position are known to typically take place on subpicosecond time scales or time scales of a few picoseconds, albeit not necessarily for all IR-active marker bands.[43] To discern the correct transient population dynamics of 7HQ upon electronic excitation of the N tautomer at early pulse delay times, the transient mid-infrared absorption bands have been analyzed using a Gaussian line shape fitting procedure (for details, see the Supporting Information). It turns out that this procedure is necessary to correctly determine the population dynamics of the A* anion that is generated in the "tight" and "loose" complexes at the early pulse delay times.

Figure 2 shows the results of our analysis of the transient population of the N* and Z* tautomer and the A* anion species in the 7HQ−imidazole reaction. The outcome of the Gaussian line shape fitting of the 1422−1430 cm^{-1} marker band of A* and of the two marker bands of Z* (1437 and 1530 cm^{-1}) is shown in panels a and b of Figure 2 for the 4.0 M imidazole case, which we have plotted on a logarithmic scale for the pulse delay *x*-axis, to accentuate the early time dynamics. Indeed, the full width at half-maximum (fwhm) of this band decreases by a factor of 2.5 within 50−100 ps (Figure 2a), which we tentatively ascribe to hydrogen bond reorganization and solvent shell rearrangement dynamics of the imidazole/imidazolium units in the 7HQ−imidazole product pairs on this time scale. Moreover, the integrated intensity of the A* marker band has a major component appearing within the time resolution, and an additional increase on the picosecond time scale (see Figure 2b). Similar early time components can also be observed in the decay of

https://doi.org/10.1021/acs.jpclett.3c00595
J. Phys. Chem. Lett. 2023, 14, 4775−4785

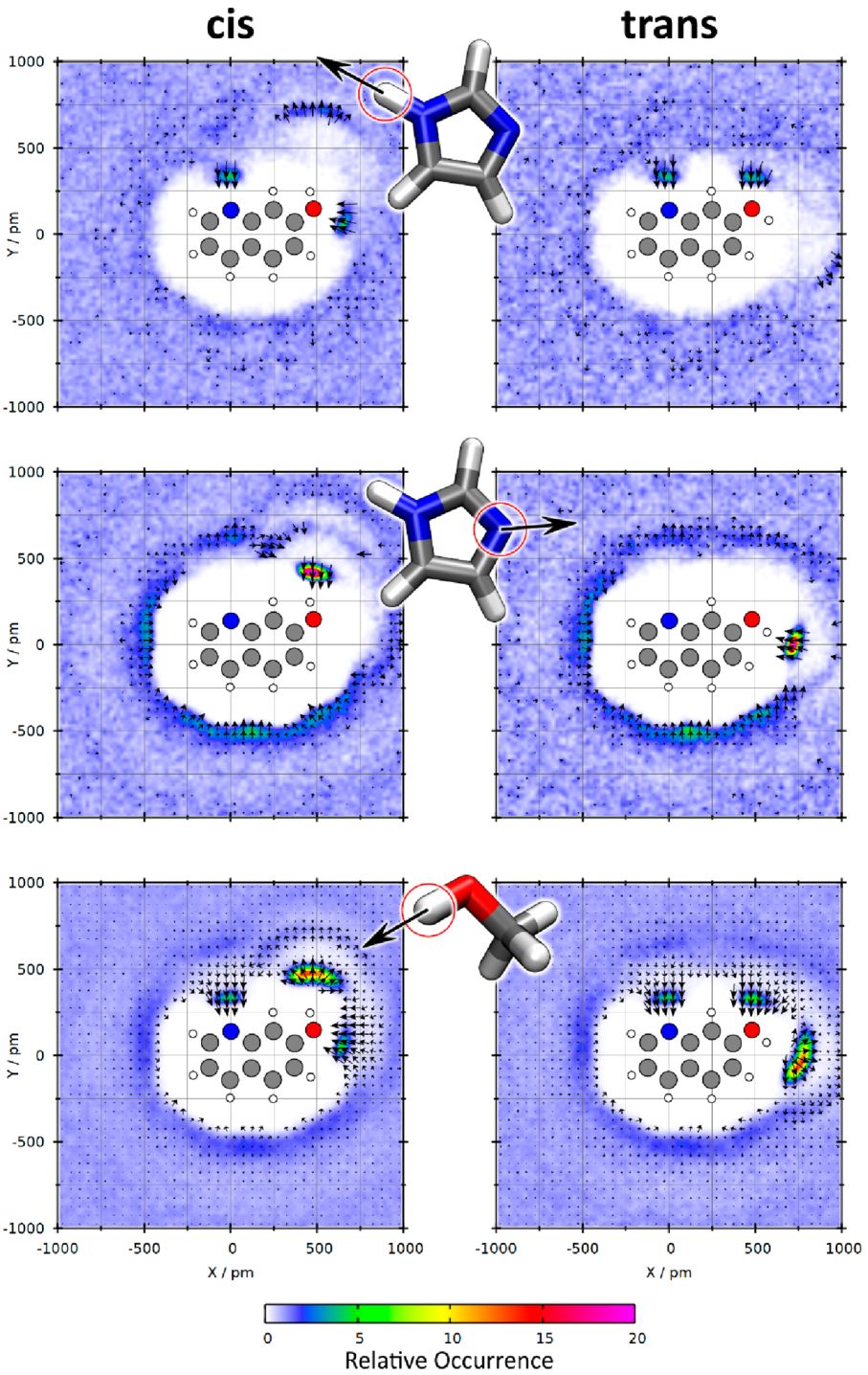

Figure 3. Average particle density of imidazole (HIm) and methanol (CH_3OH) molecules around a *cis*- or *trans*-7HQ molecule (see the color scale) together with the average orientation of the displayed vectors of HIm and CH_3OH (see the arrows).

N*, and together with the observations of the increase in the level of A*, a consistent picture of "tight" contact and "loose" solvent-separated 7HQ−imidazole reaction pairs emerges, the relative fraction for these increasing with imidazole concentration. Interestingly, at longer pulse delay times, the integrated intensity of the A* marker band decays with a time constant that appears within the error margin of the experimental data to be identical to the increase in the integrated intensity of the Z* marker band at 1530 cm^{-1} (Figure 2b). Additional components in the decay of N* occurring on a time scale of hundreds of picoseconds appear to be similar to components in the rise of Z* (Figure 2c). Results from exponential fits of these long time components are summarized in Table S2.

The experimental results clearly display a change in the reaction dynamics of 7HQ when going from 0.0 M (stock solution) to 4.0 M imidazole. The N* to Z* tautomerization accelerates in the presence of imidazole, and a switch from the solvolysis (methanolysis) "proton hole" pathway toward the protolysis "excess proton" pathway is apparent upon addition of more imidazole to the solution. To determine the relative reaction yields along these two different routes, we have used the results from the marker band fitting to Gaussian profiles

https://doi.org/10.1021/acs.jpclett.3c00595
J. Phys. Chem. Lett. 2023, 14, 4775−4785

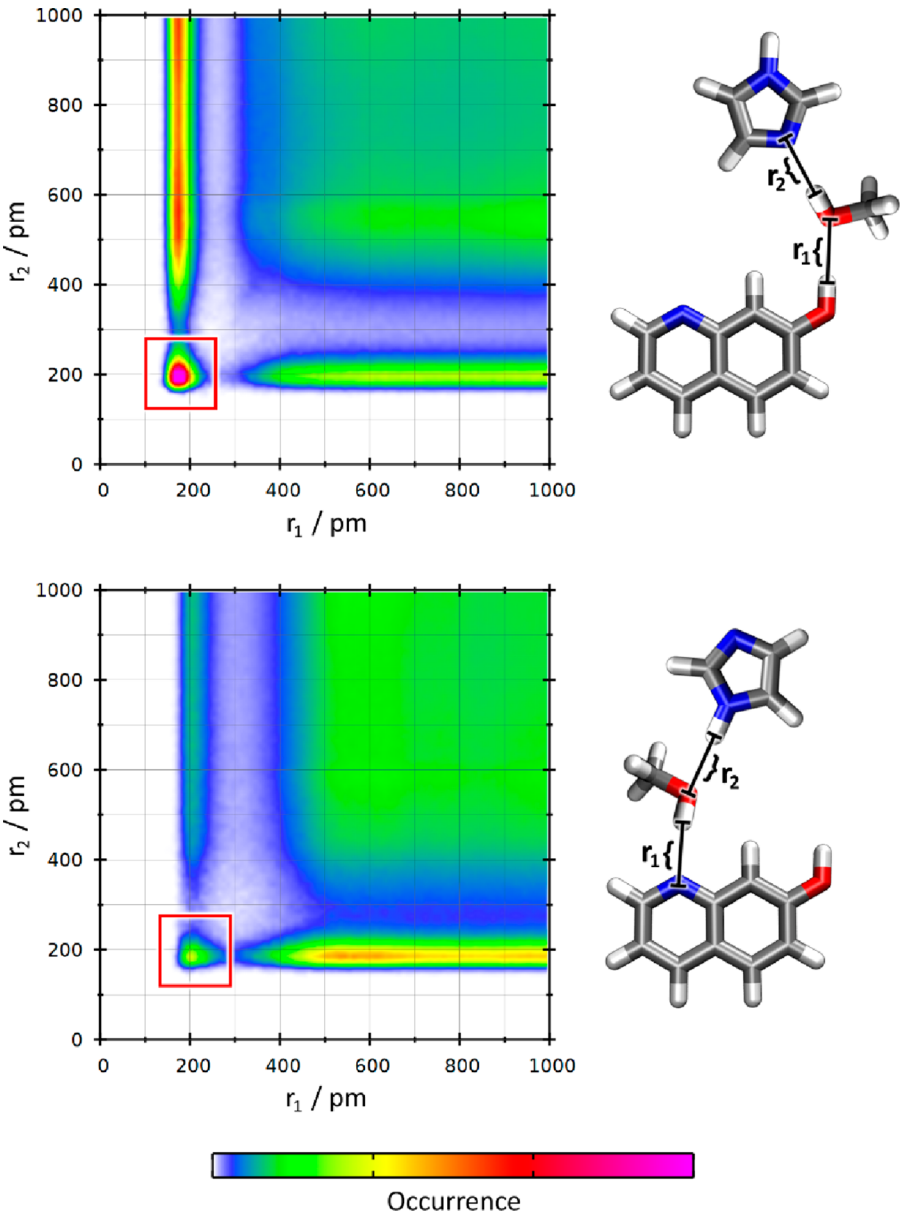

Figure 4. Combined distribution function depicting the probability of finding a certain distance (see the sketch) between 7HQ and CH_3OH and between CH_3OH and HIm on the horizontal and vertical axes, respectively.

(see also Figure S3). For the stock solution, we observe an equilibration of the fraction (f_i) of photoexcited 7HQ–N* molecules from $f_{N^*}(\tau = 0\ \text{ps}) = 1$ to $f_{N^*}(\tau = 1\ \text{ns}) = 0.35$. Realizing that for the "proton hole" pathway, with 7HQ following the N* → C* → Z* tautomerization route, only a significant transient population of the N* and Z* tautomers has been observed at any pulse delay for 7HQ in deuterated methanol (CD_3OD),[11,42,43] we can then correlate the value of the observed transient absorbance of the Z* 1540 cm^{-1} band with a transient population value: $f_{Z^*}(\tau = 1\ \text{ns}) = 0.65$ [with $f_{Z^*}(\tau = 0\ \text{ps}) = 0$]. Assuming that the IR cross sections of the integrated 7HQ marker bands are not affected when going from the (0.0 M imidazole) stock solution to 4.0 M imidazole in CD_3OD, we learn then that with a 1 ns pulse delay the fraction of Z* increases to $f_{Z^*}(\tau = 1\ \text{ns}) = 0.80 \pm 0.03$ while that of N* is much smaller [$f_{N^*}(\tau = 1\ \text{ns}) = 0.03 \pm 0.03$]. This means that the value observed for the integrated band intensity of the A* anion with a 1 ns pulse delay is significant: $f_{A^*}(\tau = 1\ \text{ns}) = 0.17 \pm 0.03$. Now comparing the long delay value of the integrated band value of A* (9.4 ± 0.2) with that of its maximum value (19.8 ± 0.2) reached at 10 ps, we learn that under 4.0 M imidazole conditions a transient population build-up fraction of A* reaches a value of $f_{A^*}(\tau = 10\ \text{ps}) = 0.36 \pm 0.07$. This value is consistent with the decrease in the transient population of N* from $f_{N^*}(\tau = 0\ \text{ps}) = 1$ to $f_{N^*}(\tau = 10\ \text{ps}) = 0.45 \pm 0.05$, due to the fast deuteron transfer reaction for "tight" and "loose" complexes, as derived from the early time decay components of the N* marker band at 1470 cm^{-1}.

The decay of the integrated area of the A* marker band at time scales of hundreds of picoseconds correlates well with the rise of that of the Z* marker band points strongly to the dominant occurrence of the N* → A* → Z* pathway at 4.0 M imidazole, yet we cannot unequivocally exclude the possibility that a significant fraction still follows the N* → C* → Z* pathway. One could interpret the long time dynamical behavior of the N*, A*, and Z* marker bands in experimental

https://doi.org/10.1021/acs.jpclett.3c00595
J. Phys. Chem. Lett. 2023, 14, 4775−4785

observations as being indicative of further fractions of the 7HQ N* tautomer following the N* → A* → Z* pathway, for which the first proton/deuteron transfer step takes more time due to rearrangements of the imidazole molecules toward the proton/deuteron-donating 7HQ−OH site with possible interstitial solvent molecules, including partial rotational and diffusional motions. After these rearrangements, a proton/deuteron transfer rate may be inferred from free energy−reactivity relationships (see Table S3), albeit this under the assumption of spherical shapes for acids and bases without explicit molecular structure, to model the long time components in diffusion-assisted photoacid−base reactions in protic solvents.[11,42,43,46−52] On the contrary, the alternative option of imidazole acting as a proton/deuteron donor toward the 7HQ−quinoline nitrogen site also must be considered. As the acidity of imidazole as a proton donor is quite similar to that of the solvent methanol, one can also argue that a major fraction of 7HQ still follows the N* → C* → Z* pathway, but now with the first step initiated by imidazole acting as proton donor forming the imidazolate anion. On the basis of our experimental results, we can exclude an ultrafast proton/deuteron transfer on subpicosecond time scales or time scales of a few tens of picoseconds for the N* → C* → Z* pathway, because C* is not observed at these short pulse delay times and Z* is only formed with a time constant of 150 ps at 4.0 M imidazole. This implies, even for 4.0 M imidazole conditions, an absence of "tight" complexes when the preexisting hydrogen bond between the 7HQ quinoline nitrogen site and N−H group of imidazole comprises a barrierless proton transfer reaction coordinate or when these "tight" complexes have a major abundance it has a major reaction barrier with a 150 ps reaction time constant as a result. To discern which of these two options prevails, we now present our results on classical molecular dynamics simulations and electronic excited state quantum chemical calculations.

More insight into the geometric aspects of specific 7HQ−imidazole reaction pair configurations can be obtained from the atomic and molecular spatial distribution functions of solvent molecules around 7HQ, which can be derived from molecular dynamics simulations. Figure 3 shows the average particle densities of methanol and imidazole around the hydrogen bond-donating and -accepting sites of 7HQ. These results show a pronounced occurrence of having the 7HQ−OH group acting as a hydrogen bond donor, for the *cis* and *trans* configurations of the hydroxyl group, to a specific methanol or imidazole molecule acting with their lone pairs as a hydrogen bond acceptor. Here it is good to note that the distribution of dihedral angle functions of 7HQ is ∼60% *cis*-7HQ and ∼40% *trans*-7HQ, irrespective of the concentration of imidazole used in our experiments. The dihedral angles have rather narrow distributions of the *cis*-7HQ and *trans*-7HQ configurations with their maxima in the plane of the 7HQ−aromatic backbone (see the Supporting Information). As a result, the spatial distribution functions of methanol and imidazole are confined to a limited range around the hydrogen bond-donating and -accepting sites of 7HQ. This fact also validates the assumption that a planar projection of the solvent distribution functions, as shown in Figure 3, provides all essential information in a transparent fashion.

The fact that the magnitudes of the calculated spatial distribution functions for methanol or imidazole being donors of hydrogen bonds to the 7HQ hydroxyl and quinoline nitrogen lone pairs are approximately 3−4 times lower than those where methanol or imidazole acts as a hydrogen bond acceptor strongly suggests an accordingly smaller hydrogen bond interaction strength for these two different types of hydrogen bonds that 7HQ can have. This also means that in the context of preformed "tight" contact reaction pairs imidazole is more likely to act with its nitrogen lone pair as a base to the 7HQ hydroxyl acidic group than imidazole is to act with its N−H group as an acid to donate the proton to the 7HQ quinoline nitrogen site. To determine whether a similar situation occurs for the "loose" solvent-separated reaction pairs, we computed the two-dimensional distribution functions from our molecular dynamics simulations (Figure 4). Here, again, a larger relative occurrence is apparent for those "loose" complexes where the solvent and imidazole are interacting as hydrogen bond acceptors to the 7HQ−OH group. Instead, in the other "loose" complexes, the solvent and imidazole act as hydrogen bond donors to the 7HQ−quinoline nitrogen. The combined distribution functions also show that the hydrogen bond distances are indicative of weak hydrogen bond strengths,[53−56] as expected for 7HQ in the electronic ground state.

The observed population kinetics obtained from the experimental ultrafast UV/IR pump−probe results shows that for high imidazole concentrations the N* → A* → Z* pathway of 7HQ is the dominant pathway for the "tight" and "loose" reaction pair fractions. The particle density and distribution functions derived strongly point to a significant fraction of imidazole being hydrogen bonded at both the 7HQ−OH and 7HQ−quinoline nitrogen sites for these "tight" and "loose" reaction pairs. These findings yield a series of new questions about the relative reaction rates for individual proton transfer steps. (1) Why is the deprotonation of N* into the solvent faster toward imidazole than toward methanol? (2) Why is the protonation of A* at the nitrogen site faster when taken from imidazole than from methanol as the proton donor? (3) Why is the protonation at the nitrogen site from imidazole faster for A* than for N*, whereas the opposite is the case for methanol?[42] To provide insight into these factors that control the reaction rates of individual steps and the overall relative importance of the N* → A* → Z* and N* → C* → Z* pathways, we have determined the proton transfer energy profiles for the distinct reaction steps for the "tight" hydrogen-bonded 7HQ−HIm complexes (see Figure 5). For the reaction path, we used a linear interpolation between the optimized reactant and product geometries. This path was sampled with vertical excitation energy calculations at the time-dependent density functional theory (TD-DFT) level. The solvent screening effect was incorporated via effective polarizable continuum methods using both the dielectric constants corresponding to electronic polarization only (ε_∞ = 4.5,[57] inspired from the observation that the protonation reaction is considerably faster than the geometric solvent reorientation dynamics) and, for comparison, the dielectric constant corresponding to full solvent relaxation (ε_0 = 32.63[58]). Special care was taken to correctly follow the proper electronic excited state energy profile (i.e., the one that corresponds to the S_1 state of 7HQ) that does not always represent the lowest vertical excitation along the reaction path. Our calculations show that from an enthalpy perspective, the imidazole molecules are considerably more likely to accept or donate a proton than are methanol molecules. The reaction barriers with methanol as the proton acceptor or donor are so much higher (on the order of 80 kJ/mol) that whenever imidazole is

https://doi.org/10.1021/acs.jpclett.3c00595
J. Phys. Chem. Lett. 2023, 14, 4775−4785

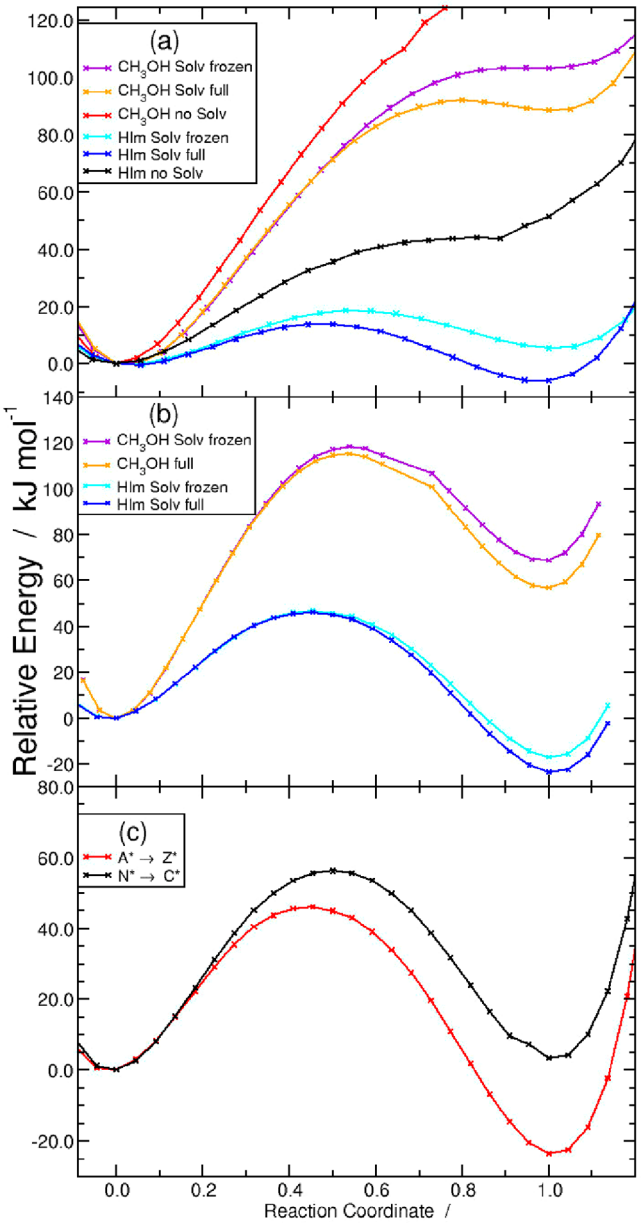

Figure 5. Energy paths for (a) oxygen site deprotonation onto HB = CH_3OH, HIm (N* + HB → A* + H_2B^+) and (b) proton abstraction from HB onto the nitrogen site (A* + HB → Z* + B^-) in both cases with different solvation influences. (c) Energy path for proton abstraction of HIm onto A* and N*.

present in the solvent, the reaction will preferentially follow those pathways where imidazole is actively involved as the proton acceptor [N* + HB → A* + H_2B^+ (Figure 5a)] or the proton donor [A* + HB → Z* + B^- (Figure 5b)]. In terms of relative reaction rates, we estimate that the reaction via imidazole will occur 10^8 times faster than via methanol, assuming that the vibrational relaxation after vertical excitation results in a locally increased kinetic energy of the proton corresponding to a proton temperature of 600 K. Finally, in the comparison of proton abstraction by either N* or A* from imidazole, it follows that the barrier of the A* + HB → Z* + B^- pathway is lower than that of the N* + HB → C* + B^- pathway (with HB being imidazole). In this case, the relative reaction rates can be estimated to differ by a factor of 50 (considering a relative barrier difference of 10 kJ/mol at a proton temperature of 300 K, as the reacting proton does not originate from 7HQ and therefore does not have an increased temperature).

A close connection between acid−base reaction rates has been defined by Marcus using the BEBO free energy−reactivity relation,[46] and ultrafast proton transfer studies have shown that this relationship appears to confirm predicted proton transfer rates with those derived from experiments.[11,49−51] The current understanding is that conclusions can be drawn about only solvent-mediated proton transfer, i.e., for "loose" solvent-separated acid−base reaction pairs. Interestingly, despite this caveat, an assessment of the acid−base reactivity of 7HQ with imidazole based on a comparison of the differences in pK_a values, ΔpK_a (see Table S3), also provides for the case of "tight" acid−base reaction pairs a clear indication of why N* reacts faster with imidazole than with methanol as the proton acceptor or why A* reacts faster with imidazole than with methanol as the proton donor and why abstraction of a proton from imidazole by A* is faster than that by N*. We argue that with the current energy barrier calculations we can provide a proper estimate in quantitative terms of the extent to which a close similarity exists between the quantum chemical calculations of acid−base reaction pairs and the semiempirical BEBO free energy relationship.

We note that the energy barriers, the ΔpK_a values, and the observed reaction rates all point to imidazole being a faster proton transporter than methanol, even though the underlying mechanisms for proton transport are similar.[10,24] We suggest that the individual steps in charge separation are more efficiently mediated by the larger aromatic imidazole both as a proton acceptor and as a proton donor (due to a greater delocalization of the charge on the imidazole cation and anion, respectively; this feature also applies for the aromatic 7HQ molecule) than by methanol where the charge is much more localized. Ultimately, our findings for the energy barriers of the individual proton transfer steps with imidazole as the proton donor and proton acceptor strongly suggest that the N* → A* → Z* pathway is followed by those 7HQ molecules that are already in the "tight" and "loose" reaction pair configurations and is the more likely route followed by those 7HQ molecules where larger orientational rearrangements are necessary before a reaction with imidazole can proceed.

We have attempted to identify the underlying reasons for the shape of the energy profiles in terms of the degree of charge delocalization in the solvent molecules (methanol and imidazole), in view of providing an intuitive qualitative answer to the three questions about the proton transfer reaction rates. For this purpose, we have computed the changes in the partial charges for the A* + HB → Z* + B^- reaction for the oxygen/nitrogen atoms of B. While for methanol the oxygen partial charge changes from −0.54 to −0.98, the imidazole nitrogen charge changes from −0.13 to −0.39. Interestingly, the other nitrogen atom in imidazole remains practically unchanged, and its partial charge changes from −0.35 to −0.39. The negative charge is thus equally shared between the two nitrogen atoms, while in CH_3O^-, the entire charge is carried by the single oxygen atom. This illustrates the considerably better intramolecular delocalization of the anionic excess charge for imidazole compared to methanol, which in turn explains why the proton donation capability is so much better for imidazole. A similar argument holds for the 7HQ deprotonation reactions. Along this line of argument, we anticipate similar effects will play an important role in proton transport in mixed

https://doi.org/10.1021/acs.jpclett.3c00595
J. Phys. Chem. Lett. 2023, 14, 4775−4785

water/imidazole and mixed methanol/imidazole solutions without the photoacid chromophore, but much less in neat imidazole or imidazole derivatives.[24,26]

In conclusion, our joint experimental−theoretical study illustrates that it is possible to manipulate the pathway of acid−base proton exchange reactions in a controlled way, exploiting the different microsolvation properties and proton affinities of suitably chosen solvent molecules. Here, we have used the bifunctional photoacid 7HQ in combination with methanol and imidazole as solvent components, as opposed to the more common aqueous solvation. In comparison to the water environment, we observe specific changes in the reaction pathways and reaction dynamics when 7HQ is transformed from the N* state to the final Z* state. Previous studies of proton transfer pathways of 7HQ in methanol have shown that the acquisition of a proton from the solvent methanol by the 7HQ quinoline nitrogen site is the first and rate-determining step followed by a fast proton donation by the 7HQ hydroxyl OH group to the solvent (with the reaction rate of the first N* → C* step being 2 orders of magnitude smaller than that of the second C* → Z* step). Adding imidazole as a reaction partner quantitatively changes the time ordering of the proton transfer steps, with ultrafast proton donation of the 7HQ hydroxyl OH group to imidazole occurring on a subpicosecond time scale or a time scale of a few picoseconds, and only at clearly longer time scales does the acquisition of a proton by the 7HQ quinoline nitrogen site from a nearby imidazole complete the 7HQ N* → Z* tautomerization reaction. The sequential N* → A* → Z* pathway has, irrespective of the 7HQ−imidazole reaction pair configurations being "tight" contact or "loose" solvent-separated, a 2−3 order of magnitude difference in reaction rates between the first N* → A* step and the second A* → Z* step. In light of our findings of this large difference in reaction rates for imidazole as the proton acceptor compared to imidazole as the proton donor, it would be interesting to further explore this aspect in those cases in which imidazole derivatives mediate proton transfer, such as in HT-PEMFC or transmembrane proton channel proteins.

EXPERIMENTAL AND COMPUTATIONAL METHODS

The Supporting Information includes details about the experimental setup used;[11,42,43] free energy−reactivity assessments (using reported[42,59,60] or derived[61−63] pK_a values); molecular dynamics simulations with LAMMPS[64] and PACKMOL[65] packages, and using optimized potentials for liquid simulations all-atom (OPLS-aa) force fields,[66] restrained electrostatic potentials (RESP),[67] and a Nosé−Hoover chain thermostat;[68−70] trajectory analysis using the TRAVIS,[71,72] VMD,[73] and Tachyon[74] program packages; and proton transfer energy profiles calculated with ORCA[58] on the TD-DFT level with a solvent polarizable continuum model (CPCM).[75]

ASSOCIATED CONTENT

Supporting Information

The Supporting Information is available free of charge at https://pubs.acs.org/doi/10.1021/acs.jpclett.3c00595.

Experimental details and computational details, steady state and transient IR spectra, examples of Gaussian line shape fits of A* and Z* marker bands, exponential fits of long time behavior kinetics, free energy−reactivity relationships, acidities and reactivities as estimated for 7HQ and imidazole in H_2O, CH_3OH, and CD_3OD solutions, and dihedral distribution functions (PDF)

AUTHOR INFORMATION

Corresponding Authors

Erik T. J. Nibbering − *Max Born Institut für Nichtlineare Optik und Kurzzeitspektroskopie, 12489 Berlin, Germany;* orcid.org/0000-0001-5874-8052; Email: nibberin@mbi-berlin.de

Daniel Sebastiani − *Institut für Chemie, Martin-Luther-Universität Halle-Wittenberg, 06120 Halle (Saale), Germany;* orcid.org/0000-0003-2240-3938; Email: daniel.sebastiani@chemie.uni-halle.de

Authors

Marius-Andrei Codescu − *Max Born Institut für Nichtlineare Optik und Kurzzeitspektroskopie, 12489 Berlin, Germany*

Thomas Kunze − *Institut für Chemie, Martin-Luther-Universität Halle-Wittenberg, 06120 Halle (Saale), Germany*

Moritz Weiß − *Institut für Chemie, Martin-Luther-Universität Halle-Wittenberg, 06120 Halle (Saale), Germany*

Martin Brehm − *Institut für Chemie, Martin-Luther-Universität Halle-Wittenberg, 06120 Halle (Saale), Germany;* orcid.org/0000-0002-6861-459X

Oleg Kornilov − *Max Born Institut für Nichtlineare Optik und Kurzzeitspektroskopie, 12489 Berlin, Germany;* orcid.org/0000-0002-3343-2614

Complete contact information is available at: https://pubs.acs.org/10.1021/acs.jpclett.3c00595

Notes

The authors declare no competing financial interest.

ACKNOWLEDGMENTS

The authors cordially acknowledge the financial support from the Deutsche Forschungsgemeinschaft (DFG) under Project 263266015 (Project codes SE 1008/11-2 and NI 492/13-2) and the European Research Council (ERC) under the European Union's Horizon 2020 research and innovation program (ERC Grant Agreement 788704). M.B. acknowledges financial support by the Deutsche Forschungsgemeinschaft (DFG) through Project Br 5494/1-3.

REFERENCES

(1) de Grotthuss, C. J. T. Sur la Décomposition de l'Eau et des Corps Qu'elle Tient en Dissolution à l'Aide de l'Électricité Galvanique. *Ann. Chim.* **1806**, *LVIII*, 54−74.

(2) von Grotthuss, T. Über die Chemische Wirksamkeit des Lichts und der Elektricität; Besonders über einen Merkwürdigen Neuen Gegensatz dieser Wirksamkeit, den das Licht auf Gewisse Substanzen Äußert, je Nachdem es entweder aus Nicht-Oxidirenden Körpern oder aus der Atmosphärischen Luft Unmittelbar in Dieselben und aus Letzteren in Jene Eindringt. *Jahresverhandlungen der Kurländischen Gesellschaft für Literatur und Kunst* **1819**, *1*, 119−194.

(3) Agmon, N. The Grotthuss Mechanism. *Chem. Phys. Lett.* **1995**, *244*, 456−462.

(4) Tuckerman, M.; Laasonen, K.; Sprik, M.; Parrinello, M. Ab-Initio Molecular-Dynamics Simulation of the Solvation and Transport of H_3O^+ and OH^- Ions in Water. *J. Phys. Chem.* **1995**, *99*, 5749−5752.

(5) Tuckerman, M.; Laasonen, K.; Sprik, M.; Parrinello, M. Ab-Initio Molecular-Dynamics Simulation of the Solvation and Transport of Hydronium and Hydroxyl Ions in Water. *J. Chem. Phys.* **1995**, *103*, 150−161.

(6) Marx, D.; Tuckerman, M. E.; Hutter, J.; Parrinello, M. The Nature of the Hydrated Excess Proton in Water. *Nature* **1999**, *397*, 601−604.
(7) Vuilleumier, R.; Borgis, D. Transport and Spectroscopy of the Hydrated Proton: A Molecular Dynamics Study. *J. Chem. Phys.* **1999**, *111*, 4251−4266.
(8) Schmitt, U. W.; Voth, G. A. The Computer Simulation of Proton Transport in Water. *J. Chem. Phys.* **1999**, *111*, 9361−9381.
(9) Marx, D. Proton Transfer 200 Years after von Grotthuss: Insights from Ab Initio Simulations. *ChemPhysChem* **2006**, *7*, 1848−1870.
(10) Morrone, J. A.; Tuckerman, M. E. Ab Initio Molecular Dynamics Study of Proton Mobility in Liquid Methanol. *J. Chem. Phys.* **2002**, *117*, 4403−4413.
(11) Ekimova, M.; Hoffmann, F.; Bekçioğlu-Neff, G.; Rafferty, A.; Kornilov, O.; Nibbering, E. T. J.; Sebastiani, D. Ultrafast Proton Transport between a Hydroxy Acid and a Nitrogen Base Along Solvent Bridges Governed by the Hydroxide/Methoxide Transfer Mechanism. *J. Am. Chem. Soc.* **2019**, *141*, 14581−14592.
(12) Andot, K.; Hynes, J. T. HCl Acid Ionization in Water - a Theoretical Molecular Modeling. *J. Mol. Liq.* **1995**, *64*, 25−37.
(13) Geissler, P. L.; Dellago, C.; Chandler, D.; Hutter, J.; Parrinello, M. Autoionization in Liquid Water. *Science* **2001**, *291*, 2121−2124.
(14) Park, J. M.; Laio, A.; Iannuzzi, M.; Parrinello, M. Dissociation Mechanism of Acetic Acid in Water. *J. Am. Chem. Soc.* **2006**, *128*, 11318−11319.
(15) Hassanali, A.; Giberti, F.; Cuny, J.; Kühne, T. D.; Parrinello, M. Proton Transfer through the Water Gossamer. *Proc. Natl. Acad. Sci. U.S.A.* **2013**, *110*, 13723−13728.
(16) Pines, D.; Ditkovich, J.; Mukra, T.; Miller, Y.; Kiefer, P. M.; Daschakraborty, S.; Hynes, J. T.; Pines, E. How Acidic Is Carbonic Acid? *J. Phys. Chem. B* **2016**, *120*, 2440−2451.
(17) Mohammed, O. F.; Pines, D.; Dreyer, J.; Pines, E.; Nibbering, E. T. J. Sequential Proton Transfer through Water Bridges in Acid-Base Reactions. *Science* **2005**, *310*, 83−86.
(18) Mohammed, O. F.; Pines, D.; Nibbering, E. T. J.; Pines, E. Base-Induced Solvent Switches in Acid-Base Reactions. *Angew. Chem., Int. Ed.* **2007**, *46*, 1458−1469.
(19) Mohammed, O. F.; Pines, D.; Pines, E.; Nibbering, E. T. J. Aqueous Bimolecular Proton Transfer in Acid-Base Neutralization. *Chem. Phys.* **2007**, *341*, 240−257.
(20) Cox, M. J.; Timmer, R. L. A.; Bakker, H. J.; Park, S.; Agmon, N. Distance-Dependent Proton Transfer Along Water Wires Connecting Acid-Base Pairs. *J. Phys. Chem. A* **2009**, *113*, 6599−6606.
(21) Thomas, V.; Rivard, U.; Maurer, P.; Bruhacs, A.; Siwick, B. J.; Iftimie, R. Concerted and Sequential Proton Transfer Mechanisms in Water-Separated Acid-Base Encounter Pairs. *J. Phys. Chem. Lett.* **2012**, *3*, 2633−2637.
(22) Rivard, U.; Thomas, V.; Bruhacs, A.; Siwick, B.; Iftimie, R. Donor-Bridge-Acceptor Proton Transfer in Aqueous Solution. *J. Phys. Chem. Lett.* **2014**, *5*, 3200−3205.
(23) Vilčiauskas, L.; Tuckerman, M. E.; Bester, G.; Paddison, S. J.; Kreuer, K.-D. The Mechanism of Proton Conduction in Phosphoric Acid. *Nat. Chem.* **2012**, *4*, 461−466.
(24) Long, Z. R.; Atsango, A. O.; Napoli, J. A.; Markland, T. E.; Tuckerman, M. E. Elucidating the Proton Transport Pathways in Liquid Imidazole with First-Principles Molecular Dynamics. *J. Phys. Chem. Lett.* **2020**, *11*, 6156−6163.
(25) Luduena, G. A.; Kuhne, T. D.; Sebastiani, D. Mixed Grotthuss and Vehicle Transport Mechanism in Proton Conducting Polymers from Ab Initio Molecular Dynamics Simulations. *Chem. Mater.* **2011**, *23*, 1424−1429.
(26) Cosby, T.; Vicars, Z.; Heres, M.; Sangoro, J. Associating Imidazoles: Elucidating the Correlation between the Static Dielectric Permittivity and Proton Conductivity. *Phys. Rev. Lett.* **2018**, *120*, 136001.
(27) Kreuer, K. D.; Fuchs, A.; Ise, M.; Spaeth, M.; Maier, J. Imidazole and Pyrazole-Based Proton Conducting Polymers and Liquids. *Electrochim. Acta* **1998**, *43*, 1281−1288.
(28) Kreuer, K.-D.; Paddison, S. J.; Spohr, E.; Schuster, M. Transport in Proton Conductors for Fuel-Cell Applications: Simulations, Elementary Reactions, and Phenomenology. *Chem. Rev.* **2004**, *104*, 4637−4678.
(29) Melchior, J. P.; Majer, G.; Kreuer, K. D. Why Do Proton Conducting Polybenzimidazole Phosphoric Acid Membranes Perform Well in High-Temperature PEM Fuel Cells? *Phys. Chem. Chem. Phys.* **2017**, *19*, 601−612.
(30) Grigorieff, N.; Ceska, T. A.; Downing, K. H.; Baldwin, J. M.; Henderson, R. Electron-Crystallographic Refinement of the Structure of Bacteriorhodopsin. *J. Mol. Biol.* **1996**, *259*, 393−421.
(31) Decoursey, T. E. Voltage-Gated Proton Channels and Other Proton Transfer Pathways. *Physiol. Rev.* **2003**, *83*, 475−579.
(32) Hu, F. H.; Luo, W. B.; Hong, M. Mechanisms of Proton Conduction and Gating in Influenza M2 Proton Channels from Solid-State NMR. *Science* **2010**, *330*, 505−508.
(33) Okada, A.; Miura, T.; Takeuchi, H. Protonation of Histidine and Histidine-Tryptophan Interaction in the Activation of the M2 Ion Channel from Influenza a Virus. *Biochemistry* **2001**, *40*, 6053−6060.
(34) Acharya, R.; Carnevale, V.; Fiorin, G.; Levine, B. G.; Polishchuk, A. L.; Balannik, V.; Samish, I.; Lamb, R. A.; Pinto, L. H.; DeGrado, W. F.; Klein, M. L. Structure and Mechanism of Proton Transport through the Transmembrane Tetrameric M2 Protein Bundle of the Influenza a Virus. *Proc. Natl. Acad. Sci. U.S.A.* **2010**, *107*, 15075−15080.
(35) Rini, M.; Magnes, B.-Z.; Pines, E.; Nibbering, E. T. J. Real-Time Observation of Bimodal Proton Transfer in Acid-Base Pairs in Water. *Science* **2003**, *301*, 349−352.
(36) Mason, S. F. The Tautomerism of N-Heteroaromatic Hydroxy-Compounds. 3. Ionisation Constants. *J. Chem. Soc.* **1958**, 674−685.
(37) Mason, S. F.; Philp, J.; Smith, B. E. Prototropic Equilibria of Electronically Excited Molecules. 2. 3-, 6-, and 7-Hydroxyquinoline. *J. Chem. Soc. A* **1968**, 3051−3056.
(38) Lee, S.-I.; Jang, D.-J. Proton Transfers of Aqueous 7-Hydroxyquinoline in the First Excited Singlet, Lowest Triplet, and Ground-States. *J. Phys. Chem.* **1995**, *99*, 7537−7541.
(39) Tokumura, K.; Natsume, M.; Nakagawa, T.; Hashimoto, M.; Yuzawa, T.; Hamaguchi, H.; Itoh, M. Time-Resolved Infrared Study of Ground-State Phototautomer Formed in the Excited-State Proton Transfer of 7-Hydroxyquinoline in Methanol. *Chem. Phys. Lett.* **1997**, *271*, 320−326.
(40) Bardez, E. Excited-State Proton Transfer in Bifunctional Compounds. *Isr. J. Chem.* **1999**, *39*, 319−332.
(41) Kwon, O.-H.; Mohammed, O. F. Water-Wire Catalysis in Photoinduced Acid-Base Reactions. *Phys. Chem. Chem. Phys.* **2012**, *14*, 8974−8980.
(42) Hoffmann, F.; Ekimova, M.; Bekçioğlu-Neff, G.; Nibbering, E. T. J.; Sebastiani, D. Combined Experimental and Theoretical Study of the Transient IR Spectroscopy of 7-Hydroxyquinoline in the First Electronically Excited Singlet State. *J. Phys. Chem. A* **2016**, *120*, 9378−9389.
(43) Codescu, M.-A.; Weiss, M.; Brehm, M.; Kornilov, O.; Sebastiani, D.; Nibbering, E. T. J. Switching between Proton Vacancy and Excess Proton Transfer Pathways in the Reaction between 7-Hydroxyquinoline and Formate. *J. Phys. Chem. A* **2021**, *125*, 1845−1859.
(44) Amoruso, G.; Taylor, V. C. A.; Duchi, M.; Goodband, E.; Oliver, T. A. A. Following Bimolecular Excited-State Proton Transfer between Hydroxycoumarin and Imidazole Derivatives. *J. Phys. Chem. B* **2019**, *123*, 4745−4756.
(45) Nibbering, E. T. J.; Fidder, H.; Pines, E. Ultrafast Chemistry: Using Time-Resolved Vibrational Spectroscopy for Interrogation of Structural Dynamics. *Annu. Rev. Phys. Chem.* **2005**, *56*, 337−367.
(46) Marcus, R. A. Theoretical Relations among Rate Constants Barriers and Brønsted Slopes of Chemical Reactions. *J. Phys. Chem.* **1968**, *72*, 891−899.
(47) Pines, E.; Fleming, G. R. Proton-Transfer in Mixed Water Organic-Solvent Solutions - Correlation between Rate, Equilibrium-

https://doi.org/10.1021/acs.jpclett.3c00595
J. Phys. Chem. Lett. 2023, 14, 4775−4785

Constant, and the Proton Free-Energy of Transfer. *J. Phys. Chem.* **1991**, *95*, 10448−10457.
(48) Pines, E. The Kinetic Isotope Effect in the Photo-Dissociation Reaction of Excited-State Acids in Aqueous Solutions. In *Isotope Effects in Chemistry and Biology*; Kohen, A., Limbach, H.-H., Eds.; CRC Taylor & Francis: Boca Raton, FL, 2006; pp 451−464.
(49) Adamczyk, K.; Prémont-Schwarz, M.; Pines, D.; Pines, E.; Nibbering, E. T. J. Real-Time Observation of Carbonic Acid Formation in Aqueous Solution. *Science* **2009**, *326*, 1690−1694.
(50) Munitz, N.; Avital, Y.; Pines, D.; Nibbering, E. T. J.; Pines, E. Cation-Enhanced Deprotonation of Water by a Strong Photobase. *Isr. J. Chem.* **2009**, *49*, 261−272.
(51) Prémont-Schwarz, M.; Barak, T.; Pines, D.; Nibbering, E. T. J.; Pines, E. Ultrafast Excited-State Proton-Transfer Reaction of 1-Naphthol-3,6-Disulfonate and Several 5-Substituted 1-Naphthol Derivatives. *J. Phys. Chem. B* **2013**, *117*, 4594−4603.
(52) Spies, C.; Shomer, S.; Finkler, B.; Pines, D.; Pines, E.; Jung, G.; Huppert, D. Solvent Dependence of Excited-State Proton Transfer from Pyranine-Derived Photoacids. *Phys. Chem. Chem. Phys.* **2014**, *16*, 9104−9114.
(53) Novak, A. Hydrogen Bonding in Solids. Correlation of Spectroscopic and Crystallographic Data. *Struct. Bonding (Berlin)* **1974**, *18*, 177−216.
(54) Hadži, D.; Bratos, S. Vibrational Spectroscopy of the Hydrogen Bond. In *The Hydrogen Bond: Recent Developments in Theory and Experiments*; Schuster, P., Zundel, G., Sandorfy, C., Eds.; Structure and Spectroscopy; North Holland: Amsterdam, 1976; Vol. *II*, pp 565−611.
(55) Mikenda, W.; Steinböck, S. Stretching Frequency vs. Bond Distance Correlation of Hydrogen Bonds in Solid Hydrates: A Generalized Correlation Function. *J. Mol. Struct.* **1996**, *384*, 159−163.
(56) Libowitzky, E. Correlation of O-H Stretching Frequencies and O-H···O Hydrogen Bond Lengths in Minerals. *Monatsh. Chem.* **1999**, *130*, 1047−1059.
(57) Liu, X. M.; Yu, J. S. Characterization of the Dielectric Properties of Water and Methanol in the D-Band Using a Quasi-Optical Spectroscopy. *Sci. Rep.* **2019**, *9*, 18562.
(58) Neese, F. Software Update: The ORCA Program System-Version 5.0. *Wiley Interdiscip. Rev.: Comput. Mol. Sci.* **2022**, *12*, e1606.
(59) Konijnenberg, J.; Ekelmans, G. B.; Huizer, A. H.; Varma, C. Mechanism and Solvent Dependence of the Solvent-Catalyzed Pseudo-Intramolecular Proton-Transfer of 7-Hydroxyquinoline in the 1st Electronically Excited Singlet State and in the Ground-State of Its Tautomer. *J. Chem. Soc. Faraday Trans. 2* **1989**, *85*, 39−51.
(60) Walba, H.; Isensee, R. W. Acidity Constants of Some Arylimidazoles and Their Cations. *J. Org. Chem.* **1961**, *26*, 2789−2791.
(61) Rived, F.; Roses, M.; Bosch, E. Dissociation Constants of Neutral and Charged Acids in Methyl Alcohol. The Acid Strength Resolution. *Anal. Chim. Acta* **1998**, *374*, 309−324.
(62) Rived, F.; Canals, I.; Bosch, E.; Rosés, M. Acidity in Methanol-Water. *Anal. Chim. Acta* **2001**, *439*, 315−333.
(63) Cox, B. G. *Acids and Bases: Solvent Effects on Acid-Base Strengths*; Oxford University Press: Oxford, U.K., 2013.
(64) Plimpton, S. Fast Parallel Algorithms for Short-Range Molecular-Dynamics. *J. Comput. Phys.* **1995**, *117*, 1−19.
(65) Martínez, L.; Andrade, R.; Birgin, E. G.; Martínez, J. M. PACKMOL: A Package for Building Initial Configurations for Molecular Dynamics Simulations. *J. Comput. Chem.* **2009**, *30*, 2157−2164.
(66) Jorgensen, W. L.; Maxwell, D. S.; Tirado-Rives, J. Development and Testing of the OPLS All-Atom Force Field on Conformational Energetics and Properties of Organic Liquids. *J. Am. Chem. Soc.* **1996**, *118*, 11225−11236.
(67) Golze, D.; Hutter, J.; Iannuzzi, M. Wetting of Water on Hexagonal Boron Nitride@Rh(111): A QM/MM Model Based on Atomic Charges Derived for Nano-Structured Substrates. *Phys. Chem. Chem. Phys.* **2015**, *17*, 14307−14316.
(68) Nosé, S. A Unified Formulation of the Constant Temperature Molecular-Dynamics Methods. *J. Chem. Phys.* **1984**, *81*, 511−519.
(69) Nosé, S. A Molecular-Dynamics Method for Simulations in the Canonical Ensemble. *Mol. Phys.* **1984**, *52*, 255−268.
(70) Martyna, G. J.; Klein, M. L.; Tuckerman, M. Nosé-Hoover Chains - the Canonical Ensemble Via Continuous Dynamics. *J. Chem. Phys.* **1992**, *97*, 2635−2643.
(71) Brehm, M.; Kirchner, B. TRAVIS - a Free Analyzer and Visualizer for Monte Carlo and Molecular Dynamics Trajectories. *J. Chem. Inf. Model.* **2011**, *51*, 2007−2023.
(72) Brehm, M.; Thomas, M.; Gehrke, S.; Kirchner, B. TRAVIS-a Free Analyzer for Trajectories from Molecular Simulation. *J. Chem. Phys.* **2020**, *152*, 164105.
(73) Humphrey, W.; Dalke, A.; Schulten, K. VMD: Visual Molecular Dynamics. *J. Mol. Graphics Model.* **1996**, *14*, 33−38.
(74) Stone, J. E. An Efficient Library for Parallel Ray Tracing and Animation. Master's Thesis, Missouri University of Science and Technology, Rolla, MO, 1998.
(75) Barone, V.; Cossi, M. Quantum Calculation of Molecular Energies and Energy Gradients in Solution by a Conductor Solvent Model. *J. Phys. Chem. A* **1998**, *102*, 1995−2001.

https://doi.org/10.1021/acs.jpclett.3c00595
J. Phys. Chem. Lett. 2023, 14, 4775−4785